

# UC Santa Cruz

## UC Santa Cruz Previously Published Works

### Title

Increasing the Dimensionality of Soft Microstructures through Injection-Induced Self-Folding.

### Permalink

<https://escholarship.org/uc/item/6hm224dn>

### Journal

Advanced materials (Deerfield Beach, Fla.), 30(38)

### ISSN

0935-9648

### Authors

Ranzani, Tommaso  
Russo, Sheila  
Bartlett, Nicholas W  
et al.

### Publication Date

2018-09-01

### DOI

10.1002/adma.201802739

Peer reviewed

# Increasing the Dimensionality of Soft Microstructures through Injection-Induced Self-Folding

Tommaso Ranzani,\* Sheila Russo, Nicholas W. Bartlett, Michael Wehner, and Robert J. Wood

Devices fabricated using soft materials have been a major research focus of late, capturing the attention of scientists and laypersons alike in a wide range of fields, from microfluidics to robotics. The functionality of such devices relies on their structural and material properties; thus, the fabrication method is of utmost importance. Here, multilayer soft lithography, precision laser micromachining, and folding to establish a new paradigm are combined for creating 3D soft microstructures and devices. Phase-changing materials are exploited to transform actuators into structural elements, allowing 2D laminates to evolve into a third spatial dimension. To illustrate the capabilities of this new fabrication paradigm, the first “microfluidic origami for reconfigurable pneumatic/hydraulic” device is designed and manufactured: a 12-layer soft robotic peacock spider with embedded microfluidic circuitry and actuable features.

The creation of functional devices from soft condensed matter has enjoyed increasing interest in the scientific and engineering communities, with examples ranging from microfluidic devices<sup>[1]</sup> to robotics.<sup>[2]</sup> Advantages of employing soft materials include low cost, ease of processing, robustness, and the possibility of impedance matching with humans and natural environments. Such features offer novel research opportunities in medicine,<sup>[3–5]</sup> macro- and micromanipulation,<sup>[6,7]</sup> exploration,<sup>[8,9]</sup> sensing,<sup>[10,11]</sup> and biomimetics.<sup>[12]</sup>

The behavior – and in particular the motion – of soft devices is fundamentally dictated by the geometry and properties of the constituent materials (i.e., unlike more traditional hinged

or bearing-based mechanisms); thus manufacturing techniques play a central role in the resulting function and must be considered throughout the design process. Molding is one of the most common techniques for manufacturing soft centimeter-scale devices.<sup>[13]</sup> However, at smaller scales, the structural complexity that can be obtained is limited by the manufacturability of the mold, thus restricting the design mostly to single degree-of-freedom (DoF) continuum bending structures.<sup>[14]</sup> 3D printing allows nearly arbitrary geometries,<sup>[15]</sup> yet the paucity of compatible soft materials and limited resolution engenders mostly static devices below the mesoscale. 4D printing has been proposed to develop dynamically evolving


structures<sup>[16]</sup> exploiting time-dependent shape shifting of 3D printed, stimuli-responsive materials. Planar manufacturing processes have also been used for fabricating soft devices across different scales, from meter-sized soft robots,<sup>[8]</sup> to millimeter scale soft microdevices.<sup>[17]</sup> Among planar processes, soft lithography enables dense packing of extremely fine features, leading to devices capable of (fluidic) computation, as widely demonstrated in the field of microfluidics.<sup>[18]</sup> However, with no means of altering the overall profile or shape, joints are undefinable and large motions are unattainable, relegating most soft lithographic devices to a purely 2D existence. To obviate these limitations, researchers have proposed ways of fabricating 3D microfluidic devices to create 3D networks<sup>[19–21]</sup> and self-assembling structures.<sup>[22]</sup> A number of manufacturing methods for developing innovative soft microdevices have also been proposed, such as hydrogel-based micropatterning,<sup>[23]</sup> electrically assisted ionoprinting,<sup>[24]</sup> and synthesis of materials responsive to light,<sup>[25]</sup> temperature and magnetic fields<sup>[26]</sup> for drug delivery systems. A magnetic biomedical microdevice fabricated through 3D printing and micromolding is presented in ref. [27].

Although the aforementioned techniques have enabled the fabrication of interesting examples of soft micro- and macro systems, we believe that the potential of soft functional devices has not yet been fully explored, especially at the meso- and microscale, where fabrication of complex soft functional structures still presents technological challenges. To clarify this concept, we can observe that complexity in current soft microstructures can take many forms: microfluidic devices can embody logic circuits,<sup>[18]</sup> soft microstructures demonstrate

Prof. T. Ranzani, Prof. S. Russo  
Department of Mechanical Engineering  
Boston University  
Boston, MA 02215, USA  
E-mail: tranzani@bu.edu

Prof. T. Ranzani, Prof. S. Russo, N. W. Bartlett, Prof. R. J. Wood  
Wyss Institute for Biologically Inspired Engineering  
Harvard John A. Paulson School of Engineering and Applied Sciences  
Harvard University  
Cambridge, MA 02138, USA

Prof. M. Wehner  
Department of Computer Engineering  
University of California Santa Cruz  
Santa Cruz, CA 95064, USA

 The ORCID identification number(s) for the author(s) of this article can be found under <https://doi.org/10.1002/adma.201802739>.

DOI: 10.1002/adma.201802739

intricate geometry,<sup>[28,29]</sup> and soft microactuators employ exotic materials and respond to diverse stimuli.<sup>[30]</sup> Here, we propose a distinction between structural and functional complexity. We define structural complexity in terms of characteristics of the static system, such as the spatial dimensionality (i.e., whether 2D or 3D), the number and diversity of materials involved, and geometric considerations (e.g., shape and minimum feature size). *Functional complexity* encompasses the dynamic aspects of the system, such as the number of DoF, the achievable motions and deformations, and any embodied computation or intelligence. Previous research has demonstrated instances of functional complexity, for example, microfluidic devices able to perform complex computational tasks. However, there are very few examples of soft microstructures that combine both structural and functional complexity. One example, the “Octobot”<sup>[31]</sup> is a two-DoF autonomous soft robot fabricated by exploiting a multistep process combining embedded 3D printing (EMB3D) and soft lithography. The EMB3D technique relies on printing functional and sacrificial ink inside an uncured matrix. The final forms as well as traces and feature sizes available with this technique present great opportunities, but are limited to form factors reachable with a printing tip (i.e.,  $\approx 75 \mu\text{m}$ ). As this example illustrates, the functional complexity of soft microstructures is limited largely by the chosen fabrication methodology. As in biology, the notion of a structure–function relationship is present in engineered devices as well, with structure being defined during fabrication. A new class of soft microstructures that demonstrate mature functional complexity necessitates an innovative manufacturing paradigm; to achieve this goal, we propose a hybrid technique that involves soft lithography to create multilayer interconnected microfluidic networks, bulk micromachining to form distinct layer geometries, a method to vary the bending plane of fluidic microactuators fabricated using a 2D process, and the ability to form stable 3D structures from 2D composites by in situ curing of polymers within the microfluidic network.

In this work, we explore a new method to increase the structural and (consequently) functional complexity of soft microstructures. By merging well-established techniques such as multilayer soft lithography and bulk micromachining, we combine the benefits of distinct fabrication techniques to create a new class of soft microstructures, which we call “microfluidic origami for reconfigurable pneumatic/hydraulic” (MORPH) systems. Previous work has demonstrated the possibility of exploiting laser cutting to release cut simple soft microactuators from an elastomeric matrix,<sup>[32]</sup> while templateless prototyping of polydimethylsiloxane microfluidic structures exploiting laser machining has also been proposed.<sup>[33]</sup> Here, we use lithographic techniques to manufacture elastomeric layers with embossed features that we then further modify by means of laser micromachining. After precision alignment and bonding of individual layers, the result is a soft laminate with embedded microfluidic circuitry and a nearly arbitrarily complex profile. Upon pressurization, chambers within the microfluidic circuitry expand to actuate portions of the laminate through pre-programmed motions. Actuation with an inert working fluid (such as air or water) permits recovery of the initial configuration upon depressurization, while the use of a phase-changing material converts deformed actuators into permanent structural

elements. Here, we refer to phase-changing materials as materials that undergo an irreversible phase transition (i.e., solidification) when exposed to specific stimuli, such as UV light or temperature. Combining both actuation strategies enables the transformation of static 2D laminates into dynamic 3D structures. To demonstrate the capabilities of such a technique, we designed and fabricated a 12-layer monolithic soft “spider” with integrated microfluidic circuitry and functional microactuators. The soft “spider” is conceived as a demonstration of the multiple capabilities and features of the presented process, and it is not designed to achieve locomotion or to carry out a specific task. An overview of this process can be seen in **Figure 1**. Please refer to the Supporting Information in the section *Fabrication and Process Characterization* for additional technical details on the process, and for the description of the characterizations performed on the different steps involved.

We analyzed the tolerances of our manufacturing method in terms of minimum achievable cut distance and distortions introduced during the process, and demonstrated minimum cutting distances of  $40 \mu\text{m}$  and misalignment errors down to  $4 \mu\text{m mm}^{-1}$  (see details in the sections *Quantitative Analysis of Minimum Cut Distance*, and *Distortion and Alignment Analysis* in the Supporting Information). In doing so, we investigated the possibility of using the laser cut path to define the motion of actuatable sections of the structure (i.e., a soft actuator). The motion of a typical bending actuator is defined by the relative bending stiffnesses of the portions of the actuator above and below the neutral axis. Referring to Figure 1j, and noting that the actuators in this case are monolithic (i.e., all of the same material, and thus all of the same elastic modulus), we see that the bending motion is defined by the relative thicknesses of the material above and below the bladder. With the membrane thickness  $m$  being the smallest dimension (i.e., smaller than the adjacent wall thickness  $d$ ), a typical actuator will bend about the  $y$ -axis. We denote this as out-of-plane bending, as the actuator bends out of the plane of its defining geometry. This behavior remains dominant until the minimum cut distance  $d$  becomes similar in magnitude to the membrane thickness  $m$ . When  $d \approx m$ , the bending axis begins to rotate, as  $m$  is no longer the actuator’s smallest dimension. Further decreasing the minimum cut distance below the membrane thickness causes the bending axis to rotate further, until  $d$  is appreciably smaller than  $m$  and the bending axis is fully about the  $z$ -axis (normal to the plane defining the actuator geometry). We call this *in-plane bending*, as the bending deformation is entirely within the plane of the actuator. To quantify this behavior, we performed visual tracking of multiple actuators varying the minimum cut distance. Figure 1k shows that indeed there is a transition from out-of-plane bending to in-plane bending as the minimum cut distance approaches and subsequently passes below the membrane thickness. Thus, we are able to program 3D actuator motion simply by choice of the 2D layer geometries (see section *Characterization of Bending Modes* in the Supporting Information, for details).

Traditional soft actuators deform in response to a stimulus (e.g., pressure change for fluidic actuators, electric field for electroactive materials), and remain in that deformed state for only as long as the input is applied. For instance, a typical bending fluidic actuator is one that is straight under

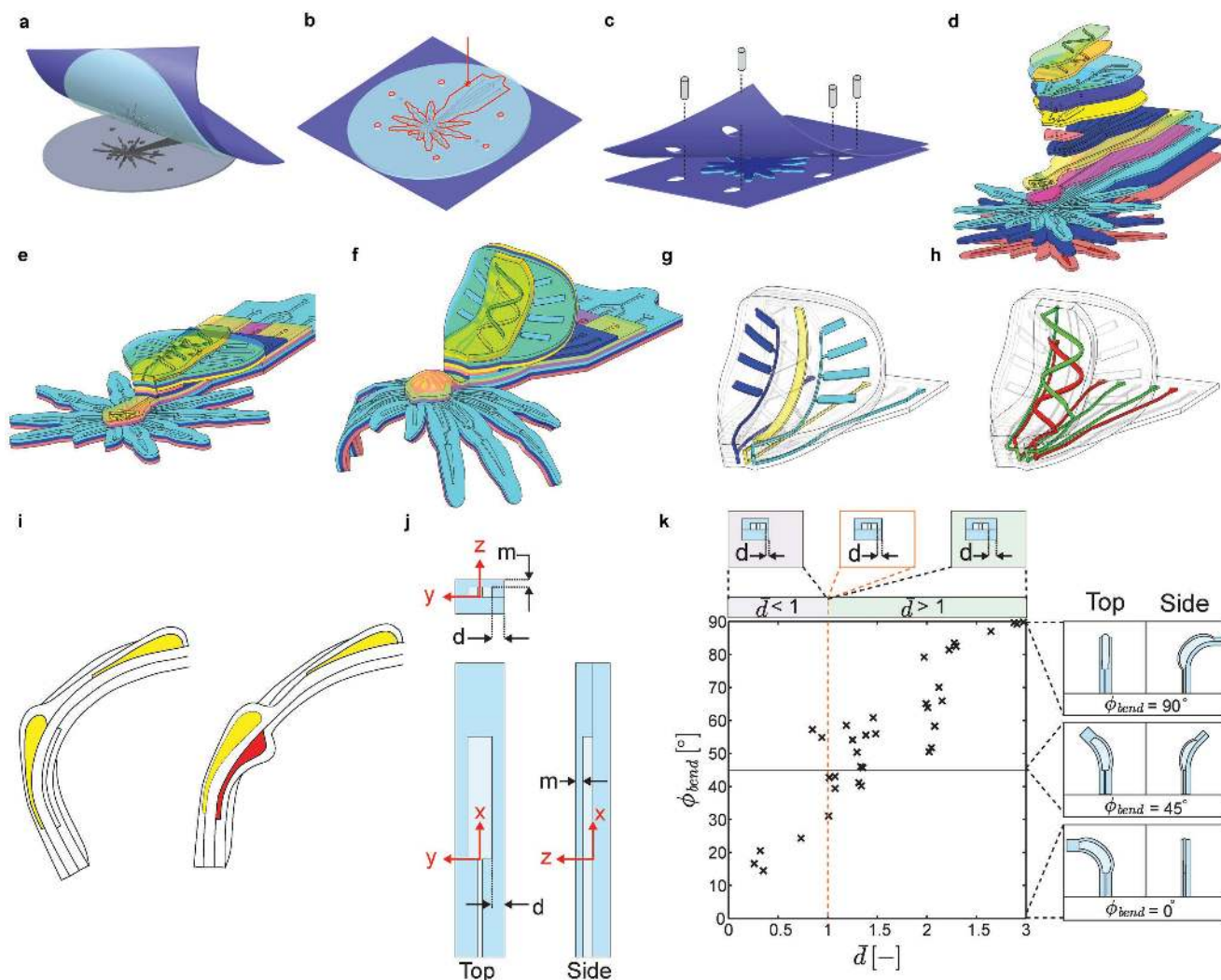


**Figure 1.** Overview of the fabrication process underlying the MORPH concept. a) Peeling a soft layer spin coated and cured on an SU-8 patterned wafer using an adhesive substrate. b) Alignment on top of the embossed features on the soft layer and laser cutting of the soft layer and associated alignment holes. c) Aligned bonding of multiple layers through surface modifications with oxygen plasma treatment; after bonding the adhesive substrate can be peeled off to allow subsequent bonding of additional layers. d) Overview of the 12 layers composing the soft spider. e) Soft spider after bonding. f) Generation of the 3D structure through the injection-induced self-folding. g) Actuation DoFs in the abdomen sublaminate. h) Microfluidic circuit in the abdomen sublaminate: path of the fluid across the multiple layers. i) Leg design: left, shape generated due to the injection of the structural DoFs (yellow); right, subsequent injection of the actuation DoF (red) to move the joint created by the structural DoF. j) Definitions of actuator coordinate system and variables from multiple views. k) Plot of bend angle as a function of normalized cut distance,  $\bar{d}$  ( $\bar{d} = d/m$ ); the final bend angle is defined as the inverse tangent of the deflection along the z-axis with respect to deflection along the y-axis. Schematics of complete out-of-plane bending ( $\varphi_{\text{bend}} = 90^\circ$ ), hybrid bending (e.g.,  $\varphi_{\text{bend}} = 45^\circ$ ), and complete in-plane bending ( $\varphi_{\text{bend}} = 0^\circ$ ) are given to the right. Above the plot is a schematic detailing the various regimes of  $\bar{d}$ .

atmospheric pressure, but bends when pressurized. When allowed to depressurize (i.e., when the input is removed), the actuator returns to its initial, undeformed state. A strategy to temporarily keep soft actuators in stable configuration was proposed in ref. [34] In contrast, we demonstrate elastomeric fluidic actuators that can be structurally locked in their deformed states through what we define as injection-induced self-folding. Instead of using traditional working fluids such as water or air, we exploit phase-changing materials to achieve this behavior. That is, we pressurize an actuator with a normally fluid material, and then solidify that material, effectively locking the entire structure in its deformed state. In this work, we

primarily use UV-curable resin as the phase-changing material, and we have also investigated the use of the uncured form of the bulk elastomer (see section *Injection with Phase-Changing Materials* in the Supporting Information for additional details on the materials tested, the process, and the properties of the injected soft laminates). Using the elastomer precursor results in a monolithic structure that is entirely soft, and also offers an alternative stimulus for structural locking (i.e., thermal curing rather than UV curing, see Supporting Information for additional details). When total recovery of the initial configuration is required, simply using an incompressible fluid (such as water) and closing an input valve would be a viable alternative.

While one could inject all microfluidic channels with a phase-changing material that is subsequently solidified, the result would be a 3D, yet entirely static structure. Far more interesting is the combination of working fluids, simultaneously locking some actuators into structural elements, while retaining other actuators to control motion.

We demonstrate the possibilities of such a scheme in a 12-layer soft peacock spider (Figure 1d–f). The complexity of the spider is best understood by individually considering the three sublaminates that compose it, each of which highlights particular benefits of this manufacturing approach. At the bottom is the leg sublaminate, which is a three-layer laminate with two sets of actuators: one embedded on the top and the other on the bottom layer. Due to their relative positions, the actuators on the first and third layers act antagonistically (Figure 1i); actuators on the first layer bend the legs up, while actuators on the third layer bend the legs down. We inject the third layer with phase-changing material, permanently deforming the legs into a bent configuration. By actuating the first layer, pressurized fluid at the joints forces the legs into a straight configuration (Figure 2a). When the pressure is relieved, the legs return to the bent configuration. This actuation strategy mimics the biomechanics of actual spiders, whose legs are bent when not actively being straightened by internal turgor pressure,<sup>[35]</sup> as is the case for the curled legs of a dead spider. The middle sublaminate contains the head and eyes. These layers collectively demonstrate the ability to achieve hierarchical structures, as the eyes are further deformations on an already deformed head. The deformation induced in the head layer leads to a change in the geometry of the channels laying on top of it (Figure 2b). The topmost sublaminate is the abdomen (Figure 2c). This sublaminate highlights multiple functionalities, including multilayer fluid handling of a microfluidic circuit, different

colored fluid patterns, and coordinated bending actuation that results in a structure with negative Gaussian curvature. The Gaussian curvature is the product of the two principal curvatures; here, we have a combination of the positive curvature induced by the elevation DoF (in the abdomen sublaminates), in yellow in Figure 1g, and the negative curvature due to the simultaneous actuation of the two flexing actuators (in the abdomen sublaminates), in dark and light blue in Figure 1g, thus producing a structure with negative Gaussian curvature. In this structure, we also demonstrate the use of laser cutting on top of channels embossed in the soft layers to allow flow across the laminate. The laser cutting step allows the user to interconnect channels across layers in 3D, allowing fluids to move “vertically” through the laminate in an analogous manner as electrical vias in printed circuit boards. We do this by strategically laser cutting holes on each soft layer individually (after realignment to the embossed fiducials and before assembly) to interconnect the channels (embossed on each layer composing the laminate) in the 3D once the layers are bonded together, again resembling a similar role as vias in printed circuit boards. This feature is particularly significant in the abdomen sublaminates, as we are able to pass the fluid through seven intermediate layers.

Mimicking the behavior of the peacock spider, three sets of independent actuators are responsible for the abdomen movement: one elevating actuator raises the abdomen from a flat to a lifted configuration (in yellow in Figure 1g) and two flexing actuators bend the abdomen outward (in dark and light blue in Figure 1g). To demonstrate colored fluid patterns and imitate the colorful abdomen of the animal, a pattern resembling the symbol of DNA is integrated on top of this sublaminate and colored fluid is injected through the 3D network of channels created by the combination of laser cut vias and microfluidic

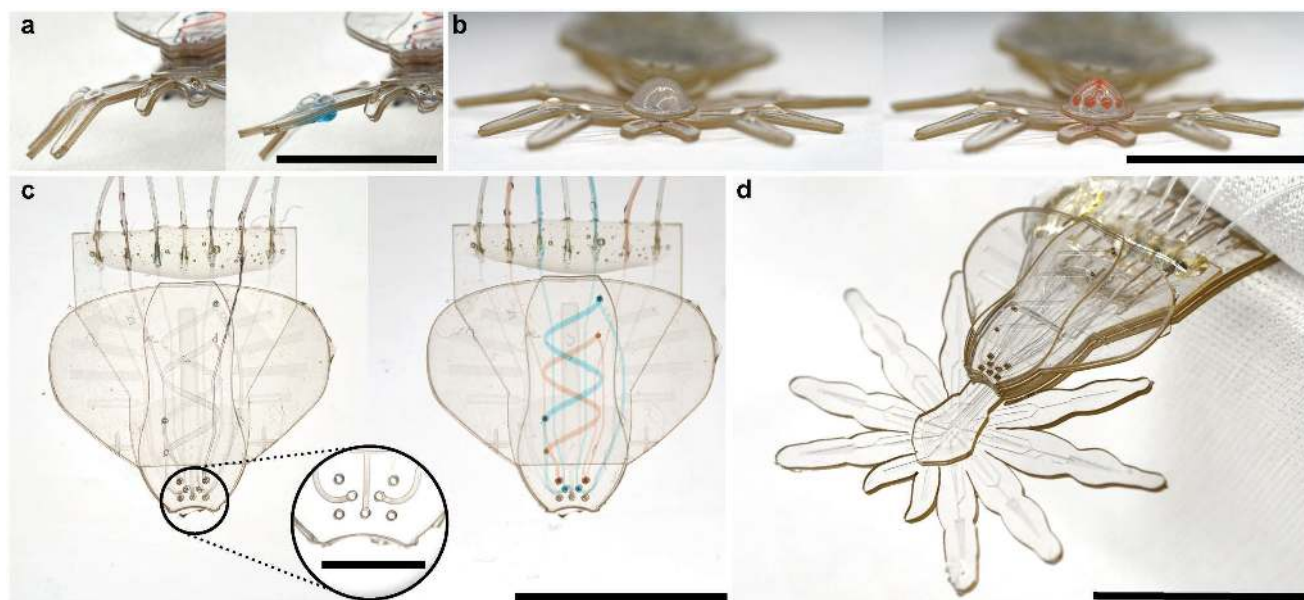


**Figure 2.** Overview of the spider structure and features. a) Detail of the legs after the injection of the structural DoFs (left) and subsequent pressurization of the actuation DoF with blue dyed water (right). b) Injection of the head (left) and subsequent coloring of the channels of the eyes (right). c) Abdomen sublaminates before (left) and after (right) coloring the two patterns that create the DNA symbol; inset: detail of the aligned features across the multiple layers. d) Fully assembled spider. Scale bar scale is 10 mm, except for inset in (c) where it is 2 mm.

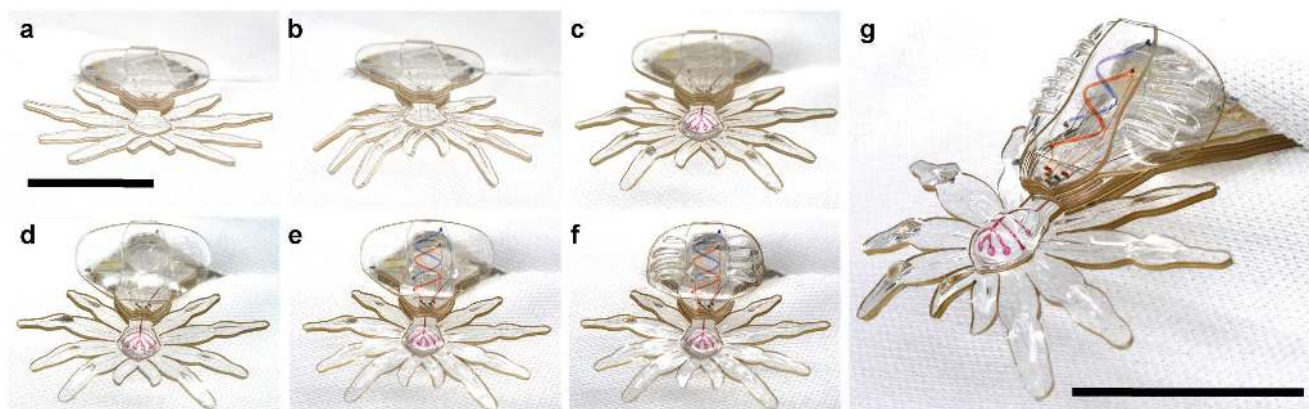


**Figure 3.** Sequence of injections that assemble and actuate the spider demonstration (Movies S1 and S2, Supporting Information). a) Flat configuration post lamination. b) Legs after structural DOF inflation: hips, left and right knees, and chelicerae (jaws). c) Head injection and coloring of the microfluidic channels of the eyes. d) Actuation of the elevation DoF on the abdomen. e) Coloring of the DNA pattern by flowing dyed water in the microfluidic circuit. f) Actuation of both the flexing DoFs on the abdomen. g) Isometric view of the 3D spider with the abdomen DoFs active. Scale bar is 10 mm.

channels (Figure 1h). The circuit is designed to be open and double ended, to demonstrate the possibility of continuously exchanging colors, as shown in Video S1 in the Supporting Information.

When assembled together, these three sublaminates make up a full MORPH system composed of 12 layers individually cut and collectively assembled (Figure 2d). The device has nine independently controllable DoFs and five structural DoFs. The sequence of injection of the structural DoFs is reported in Figure 3a–c and in Movie S1 in the Supporting Information. Additional details on the design and assembly of the device are reported in the Supporting Information, while demonstrations of the device functionalities are presented in the Movies S1–S5, Supporting Information).

The overall size of the device is 25 mm in width and the minimum feature size is 40  $\mu\text{m}$  (height of the microfluidic channels). The thickness of the soft laminate in the flat configuration is  $\approx 2.8$  mm and the spider reaches a height of  $\approx 20$  mm upon injection of phase-changing materials in the leg sublimate and injection of the abdomen elevating actuator. Structurally, this fully 3D multimaterial soft system features an intricate profile and internal geometry consisting of feature sizes that, taking advantage of the scalability of current soft lithographic techniques, may extend to the nanoscale. Functionally, the spider is highly reconfigurable, with nine individual DoFs to control motion in multiple distinct directions, and incorporates a multilayer microfluidic circuit with a 3D channel network that, in a future expansion of this process, could be used to perform electrically analogous fluidic computation. Future efforts will be targeted to use this technology to design functional robotic devices able to address specific challenges in areas such as surgical robotics, micromanipulation, and wearable devices.

The framework demonstrated here provides an example device in the form of a peacock spider showing the first steps into truly 3D soft meso- and microdevices with embedded microfluidic circuitry. This demonstration of the novel MORPH technique opens the door to a wide range of soft devices able to perform complex tasks in unstructured real-world environments. Leveraging the extensive work already done in many areas of traditional microfluidics, future 3D microfluidic devices

could include a fluidic computation unit with appendages probing the environment to sense the presence of chemicals or other phenomena of interest such as fluid flow, vibration, light, etc. In addition, this technology could also benefit from recent efforts in developing untethered soft robotic devices.<sup>[36]</sup> One can envision 3D microfluidic devices traversing complex terrains found in nature, urban settings, and even inside the human body.

## Experimental Section

Soft layers were manufactured using soft lithography. Patterned silicon wafers (3 in., (1 0 0), virgin test grade, boron-doped, p-type silicon wafers, ID:447, University Wafer) were prepared (height of features is 40  $\mu\text{m}$ ) with SU-8 2050 photoresist (MicroChem Corp.). Wafers were placed in an evacuated chamber with an open vessel containing a few drops of trichloro(1H, 1H, 2H, 2H-perfluorooctyl)silane (Sigma Aldrich) for at least 3 h. Sylgard 184 (Dow Corning) and MED4-4220 (NuSil Technology LLC) were mixed with a planetary mixer (Thinky ARE-310) poured, respectively, onto blank and patterned wafers, and degassed for 5 min in a vacuum chamber at  $-100$  kPa. Subsequently, the wafers were rotated at different speeds. Layers made of Sylgard 184 were mixed at the standard 10:1 ratio (base:curing agent), degassed, and spin coated at 350 rpm for 100 s, resulting in 300  $\mu\text{m}$  thick layers, which were then cured at 60  $^{\circ}\text{C}$  for at least 2 h. Layers made of MED4-4220 were mixed at the standard 1:1 ratio and diluted 20% w/w with a solvent (OS-2 Silicone Cleaner and Surface Prep Solvent, Dow Corning). The mixture was then degassed and spin coated at 405 rpm for 100 s, resulting in 260  $\mu\text{m}$  thick layers. After this they were left at room temperature for 12 h, and finally cured at 60  $^{\circ}\text{C}$  for at least 1 h. Soft layers were peeled off from the SU-8 patterned silicon wafer using an adhesive substrate or carrier (Gel-Pak 8 film, Gel-Pak<sup>®</sup>). Subsequently, the elastomer was cut using a precision laser micromachining system according to a specific design pattern after alignment to fiducials defined during soft lithography. Alignment holes were laser cut through the carrier to be used for future pin alignment. Layers were realigned and bonded together using  $\text{O}_2$  plasma (35 W for 30 s) treatment (Pico BR PCCE 7", Diener electronic GmbH + Co. KG). Flexible tubing, with an internal diameter of 0.254 mm (Micro Renathane Catheter Tubing, Braintree Scientific, USA), was inserted into the microchannels in the distal end of the device and sealed (Poxypak, Loctite, USA). Structural DoFs were obtained by injecting UV-curable resin (SR-355, di-trimethylolpropane tetraacrylate, Sartomer) mixed with a photoinitiator (Esacure KTO 46, Lamberti SpA).

UV exposure was performed with a UV Exposer (OAI Model 30 UV Light Source), with a measured exposure power of 19.5 mW cm<sup>-2</sup> at 365 nm.

## Supporting Information

Supporting Information is available from the Wiley Online Library or from the author.

## Acknowledgements

The authors gratefully acknowledge support from DARPA (award # FA8650-15-C-7548); the Wyss Institute for Biologically Inspired Engineering; and the Army Research Office, National Defense Science and Engineering Graduate (NDSEG) Fellowship. Any opinions, findings, conclusions, or recommendations expressed in this material are those of the authors and do not necessarily reflect those of the funding organizations. Additionally, the authors thank Neel D. Doshi for his aid in visual tracking and 3D reconstruction of actuator motions, and Eliza R. Grinnell for her help with capturing digital photographs and videos.

## Conflict of Interest

The authors declare no conflict of interest.

## Keywords

advanced manufacturing, microfluidics, soft robotics

Received: April 29, 2018

Revised: July 4, 2018

Published online: August 6, 2018

- [1] S. K. Sia, G. M. Whitesides, *Electrophoresis* **2003**, *24*, 3563.
- [2] D. Rus, M. T. Tolley, *Nature* **2015**, *521*, 467.
- [3] S. N. Bhatia, D. E. Ingber, *Nat. Biotechnol.* **2014**, *32*, 760.
- [4] T. Ranzani, G. Gerboni, M. Cianchetti, A. Menciassi, *Bioinspiration Biomimetics* **2015**, *10*, 035008.
- [5] S. P. Lacour, G. Courtine, J. Guck, *Nat. Rev. Mater.* **2016**, *1*, 16063.
- [6] J.-P. Hubschman, J.-L. Bourges, W. Choi, A. Mozayan, A. Tsirbas, C.-J. Kim, S.-D. Schwartz, *Eye (London, U. K.)* **2010**, *24*, 364.
- [7] S. Konishi, S. Shimomura, S. Tajima, Y. Tabata, *Microsyst. Nanoeng.* **2016**, *2*, 15048.
- [8] M. T. Tolley, R. F. Shepherd, B. Mosadegh, K. C. Galloway, M. Wehner, M. Karpelson, R. J. Wood, G. M. Whitesides, *Soft Rob.* **2014**, *1*, 213.
- [9] E. W. Hawkes, L. H. Blumenschein, J. D. Greer, A. M. Okamura, *Sci.* **2017**, *2*, eaan3028.
- [10] H. Zhao, K. O. Brien, S. Li, R. F. Shepherd, *Sci. Rob.* **2016**, *1*, aai7529.
- [11] A. Koh, D. Kang, Y. Xue, S. Lee, R. M. Pielak, J. Kim, T. Hwang, S. Min, A. Banks, P. Bastien, M. C. Manco, L. Wang, K. R. Ammann, K.-I. Jang, P. Won, S. Han, R. Ghaffari, U. Paik, M. J. Slepian, G. Balooch, Y. Huang, J. A. Rogers, *Sci. Transl. Med.* **2016**, *8*, 366ra165.
- [12] T. Umedachi, V. Vikas, B. Trimmer, *Bioinspiration Biomimetics* **2016**, *11*, 025001.
- [13] B. Mosadegh, P. Polygerinos, C. Keplinger, S. Wennstedt, R. F. Shepherd, U. Gupta, J. Shim, K. Bertoldi, C. J. Walsh, G. M. Whitesides, *Adv. Funct. Mater.* **2014**, *24*, 2163.
- [14] B. Gorissen, D. Reynaerts, S. Konishi, K. Yoshida, J.-W. Kim, M. De Volder, *Adv. Mater.* **2017**, *29*, 1604977.
- [15] R. L. Truby, J. A. Lewis, *Nature* **2016**, *540*, 371.
- [16] A. Sydney Gladman, E. A. Matsumoto, R. G. Nuzzo, L. Mahadevan, J. A. Lewis, *Nat. Mater.* **2016**, *15*, 413e8, <https://doi.org/10.1038/nmat4544>.
- [17] S. Rosset, H. R. Shea, *Appl. Phys. Rev. Sept.* **2016**, *3*, 031105.
- [18] S. R. Quake, *Science* **2000**, *290*, 1536.
- [19] D. Theriault, S. R. White, J. A. Lewis, *Nat. Mater.* **2003**, *2*, 265.
- [20] H. Wu, T. W. Odom, D. T. Chiu, G. M. Whitesides, *J. Am. Chem. Soc.* **2003**, *125*, 554.
- [21] K. C. Bhargava, B. Thompson, N. Malmstadt, *Proc. Natl. Acad. Sci. U. S. A.* **2014**, *111*, 15013.
- [22] M. Jamal, A. M. Zarafshar, D. H. Gracias, *Nat. Commun.* **2011**, *2*, 527.
- [23] G. H. Kwon, J. Y. Park, J. Y. Kim, M. L. Frisk, D. J. Beebe, S. H. Lee, *Small* **2008**, *4*, 2148.
- [24] E. Palleau, D. Morales, M. D. Dickey, O. D. Velev, *Nat. Commun.* **2013**, *4*, 2257.
- [25] M. Rogoz, H. Zeng, C. Xuan, D. S. Wiersma, P. Wasylczyk, *Adv. Opt. Mater.* **2016**, *4*, 1689.
- [26] J. C. Breger, C. Yoon, R. Xiao, H. R. Kwag, M. O. Wang, J. P. Fisher, T. D. Nguyen, D. H. Gracias, *ACS Appl. Mater. Interfaces* **2015**, *7*, 3398.
- [27] T. Qiu, T. C. Lee, A. G. Mark, K. I. Morozov, R. Münster, O. Mierka, S. Turek, A. M. Leshansky, P. Fischer, *Nat. Commun.* **2014**, *5*, 5119.
- [28] Y. Liu, J. Genzer, M. D. Dickey, *Prog. Polym. Sci.* **2016**, *52*, 79.
- [29] Y. Zhang, F. Zhang, Z. Yan, Q. Ma, X. Li, Y. Huang, J. A. Rogers, *Nat. Rev. Mater.* **2017**, *2*, 17019.
- [30] L. Hines, K. Petersen, G. Z. Lum, M. Sitti, *Adv. Mater.* **2016**, *1603483*.
- [31] M. Wehner, R. L. Truby, D. J. Fitzgerald, B. Mosadegh, G. M. Whitesides, J. A. Lewis, R. J. Wood, *Nature* **2016**, *536*, 451.
- [32] S. Russo, T. Ranzani, C. J. Walsh, R. J. Wood, *Adv. Mater. Technol.* **2017**, *1700135*.
- [33] H.-B. Liu, H.-Q. Gong, *J. Micromech. Microeng.* **2009**, *19*, 037002.
- [34] L. Hines, K. Petersen, M. Sitti, *Adv. Mater.* **2016**, *28*, 3690.
- [35] S. Landkammer, F. Winter, D. Schneider, R. Hornfeck, *Robotics* **2016**, *5*, 15.
- [36] S. I. Rich, R. J. Wood, C. Majidi, *Nat. Electron.* **2018**, *1*, 102.